Available online at www.sciencedirect.com

ScienceDirect

Energy Procedia 148 (2018) 503–510

Energy Procedia

www.elsevier.com/locate/procedia

A Lumped Parameter Model for the Analysis of Dynamic Effects in Wells Turbines

Irene Virdis[a], Tiziano Ghisu[a,*], Francesco Cambuli[a], Pierpaolo Puddu[a]

[a]*Dipartimento di Ingegneria Meccanica, Chimica e dei Materiali, Università di Cagliari, 09123 Cagliari, Italy*

Abstract

Breakwater integrated OWC/turbine systems are among the most well-known devices for wave energy conversion, thanks to the low environmental impact and costs of realization. These systems have been largely studied both experimentally and numerically, focusing either on OWC hydrodynamic or power unit performance. The turbine has been studied in experimental facilities that usually reproduced the periodic motion of the water column in the chamber by an artificially moved piston. Detailed studies highlighted a difference between turbine performance during piston acceleration and deceleration, usually attributed to a hysteretic behavior of the turbine. On the contrary, OWC performance has been generally studied either neglecting or crudely simplifying the turbine interaction. Numerical analyses on OWC systems, due their large scale, are often conducted using lumped parameter models, simplifying the effect of the turbine and therefore the bidirectional link between water column and turbine. The objective of this work is to introduce a lumped parameter model, able to reproduce the interaction of the turbine with the mass of air in the OWC chamber. The results of the proposed model are compared with experimental data and CFD analyses, and demonstrate that the hysteresis is caused by compressibility effects in the air chamber and not, as previously assumed, by a hysteresis in the turbine aerodynamics. The lumped parameter model allows to rapidly isolate the parameters with the largest influence on system performance, and could be integrated with existing zero-dimensional OWC models to improve to understanding of the hydrodynamic/aerodynamic interaction in the overall system.

Keywords: Wells turbine, Lumped Parameters Model, OWC, Hysteresis

1. Introduction

Oscillating Water Column (OWC) systems are among the most investigated devices for sea wave energy capture. They are combined with a Power-Take-Off (PTO) unit to transform the captured pneumatic energy into mechanical energy available on a shaft. The most common PTO is the Wells turbine, a rotor with symmetric blades that combines simplicity of operation and reliability, at the price of a narrow operating range and limited efficiency. Its performance has been studied extensively both experimentally and numerically. A large number of works focused on steady analyses by submitting the turbine to a constant flow of air in ad-hoc experimental tunnels [1, 2, 3], while others studied its dynamic performance by coupling the turbine to a large chamber where the movement of a piston

*Corresponding author. E-mail: t.ghisu@unica.it

10.1016/j.egypro.2018.08.126

reproduced the displacement of the water/air interface in the real OWC [4, 5, 6]. CFD simulations have been used both for steady [7, 8, 9, 10] and dynamic turbine performance analysis [11, 12, 13], always neglecting (even in dynamic simulations) the contribution of the large chamber used to produce the alternating flow through the turbine.

The results of experimental studies under dynamic operation (in piston-operated laboratory devices) [6] highlighted a difference in performance when turbine aerodynamic forces were reported as a function of a flow coefficient evaluated based on piston speed, during acceleration and deceleration (i.e. increasing and decreasing mass-flow). This phenomenon is usually referred to as the *hysteresis* of Wells turbines. Paderi *et al.* [14] and Puddu *et al.* [15] noticed how the experimental setup used in the experiments can cause a delay between piston movement and turbine mass-flow, concluding that, to avoid any misinterpretation in the origin of the hysteresis, turbine forces need to be reported as a function of flow conditions in the vicinity of the rotor, rather than at the piston.

In parallel, the generally accepted explanation reached by means of CFD analyses [11, 12, 13] has been questioned by Ghisu *et al.* [16, 17, 18, 19, 20], who explained how in dynamic simulations an insufficient temporal discretization can lead to a phase error that has often been confused [11, 12, 13] with the hysteresis reported in previous experimental analyses. By simulating the complete experimental setup (moving piston, air chamber and turbine), Ghisu *et al.* proved how the hysteresis is caused by compressibility effects within the air chamber (i.e. a phase delay between piston speed and turbine mass-flow) and not by an aerodynamic hysteresis of the turbine, which is very unlikely to exist at the non-dimensional frequencies Wells turbines operate at [21].

OWC performance has often been studied with lumped parameter models (LPM), obtained by solving conservation laws in integral form in control volumes appropriately selected within the system. In these analyses, the presence of the turbine is usually simplified, with the effect the bidirectional link between OWC and Wells turbine is overlooked.

The aim of this work is to study the OWC system/turbine dynamic interaction. A lumped parameter model is derived by applying mass and momentum conservation equations to air chamber and turbine duct. With an appropriate rearrangement of the equations, it is shown how the system behaves as a second order system (mass-spring-damper), where the moving piston represents the dynamic forcing and the turbine acts as the damper. An analytic solution, after linearization, is presented, and shows how this simple analysis is able to reproduce with remarkable accuracy the experimental data of Setoguchi *et al.* [6] and the CFD results obtained by Ghisu *et al.* [17]. The fact that a LPM is able to reproduce the famous hysteresis is a further evidence of its origin: compressibility within the OWC chamber and not aerodynamic effects of the turbine. The model, given its simplicity, can be easily integrated in more complete OWC analyses to provide a better prediction of the turbine interaction with the system.

Nomenclature

a	speed of sound	s^*	Laplace variable	ρ	air density
A	cross area	t	time	ρ^*	non-dimensional density
c	blade chord	t^*	non-dimensional time	σ	turbine solidity
c_x	turbine axial force coeffient	T	turbine torque	ξ	phase shift
$c_{x,\phi}$	slope of the c_x vs. ϕ_l curve	T	air temperature	ζ	damping ratio
f	frequency	T^*	torque coefficient	**Subscripts**	
F	turbine aerodynamic force	U	blade speed	f	turbine duct inlet section
G	transfer function	V	absolute velocity	a	turbine duct outlet section
h_1	air chamber height	ΔP	turbine pressure drop	0	amplitude
j	imaginary unit	Δt^*	non-dimensional time step	1	air chamber
k	non-dimensional frequency	γ	ratio of specific heats	2	turbine duct
L	turbine duct length	ϕ_p	theoretical flow coefficient	x	axial direction
M_1	mass of air in the chamber	ϕ_l	local flow coefficient	t	tangential direction
P^*	pressure drop coefficient	ω	turbine rotational speed	p	piston
r_m	blade midspan radius	Ω	piston angular frequency		
R	gas constant	Ω_n	angular natural frequency		

2. Methodology

The mutual interaction between air mass inside the chamber and Wells turbine has been studied experimentally in laboratory devices that replaced the water column inside the chamber with a mechanical piston [6]. This work uses the same geometric parameters and operating conditions of [6]. A scheme of the setup has been reported in table 1, with a detailed list dimensions and operating conditions. The non-dimensional frequency is calculated as $k = \frac{f\pi c}{U} = 1.2 \times 10^{-3}$, where f represents the frequency and U the blade speed. k is calculated with the same equation used for oscillating (pitching or plunging) airfoils, where a significantly larger value is required to produce noticeable dynamic effects [21].

Table 1: Wells turbine data and control volume scheme

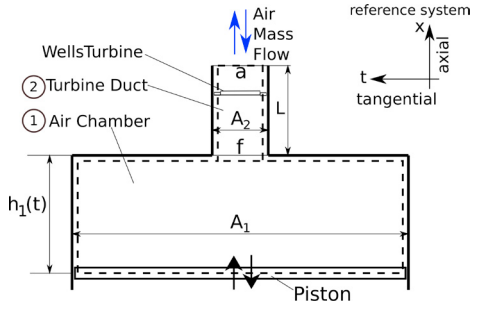

chamber diameter	1.4 m
rotor tip diameter	300 mm
rotor hub diameter	210 mm
tip clearance	1 mm
chord length c	90 mm
blade number	5,6,7
solidity at tip radius σ	0.48-0.57-0.67
sweep ratio	0.417(15/36)
rotational speed	2500 rpm
piston frequency f	6 s
turbine non-dimensional frequency k	1.2E-3

The laws of conservation of mass and axial momentum have been applied to the air volume in the chamber (control volume ① in Table 1) and to the turbine duct (control volume ②).

$$\begin{cases} \dfrac{\mathrm{d}M_1}{\mathrm{d}t} = h_1 A_1 \dfrac{\mathrm{d}\rho_1}{\mathrm{d}t} + \rho_1 A_1 \dfrac{\mathrm{d}h_1}{\mathrm{d}t} = -\rho_a V_2 A_2 \\ \dfrac{\mathrm{d}(\rho_2 V_2 A_2 L)}{\mathrm{d}t} = (p_1 - p_a)A_2 + F_x \end{cases} \tag{1}$$

The rate of variation in the mass of air in the chamber is equal to the mass-flow leaving the control volume through the opening, while the rate of momentum in the turbine duct is equal to the forces acting on the air mass it contains, which is the sum of pressure forces on the boundaries and aerodynamic forces on the turbine (F_x). Compressibility of air within the turbine duct (but not in the overall system) has been neglected ($\rho_f = \rho_a = \rho_2$), with the result that the mass-flow in any section of the turbine duct is assumed constant. Forces due to friction on the duct walls have been considered negligible with respect to aerodynamic forces acting on the turbine.

Wells turbine performance is represented in terms of non-dimensional coefficients of pressure drop P^* and torque T^*, as a function of flow coefficient ϕ, which in the experiment of Setoguchi [6] is calculated based on piston speed.

$$P^* = \frac{\Delta P}{\rho\omega^2 {r_m}^2}; \quad T^* = \frac{T}{\rho\omega^2 {r_m}^5}; \quad \phi_p = \frac{V_p}{\omega r_m}\frac{A_1}{A_2}; \tag{2}$$

The equations in (1) can be written in non-dimensional form, by dividing the mass conservation equation by $(\rho_a \omega r_m A_2)$ and the momentum equation by $(\rho_a (\omega r_m)^2 A_2)$:

$$\begin{cases} \dfrac{h_1}{r_m}\dfrac{A_1}{A_2}\dfrac{\mathrm{d}(\rho_1/\rho_a)}{\mathrm{d}(t\omega)} + \dfrac{\rho_1}{\rho_a}\dfrac{A_1}{A_2}\dfrac{\mathrm{d}(h_1/r_m)}{\mathrm{d}t} = -\dfrac{V_2}{\omega r_m} \\ \dfrac{L}{r_m}\dfrac{\mathrm{d}(V_2/(\omega r_m))}{\mathrm{d}(t\omega)} = \dfrac{(p_1 - p_a)}{\rho_a(\omega r_m)^2} + \dfrac{F_x}{\rho_a(\omega r_m)^2 A_2} \end{cases} \tag{3}$$

Introducing the following non-dimensional parameters:

$$\frac{A_1}{A_2}\frac{\mathrm{d}(h_1/r_m)}{\mathrm{d}(t\omega)} = -\phi_p \qquad \frac{V_2}{\omega r_m} = \phi_l \qquad \frac{p_1 - p_a}{\rho_a(\omega r_m)^2} = P^*$$

$$\frac{\rho_1}{\rho_a} = \rho^* = \frac{\gamma(\omega r_m)^2}{a^2}P^* + 1 \qquad \frac{F_x}{\rho_a(\omega r_m)^2 A_2} = c_x \qquad t\,\Omega = \frac{t\omega}{\omega/\Omega} = t^*$$

equation (3) becomes:

$$\begin{cases} \dfrac{h_1 A_1 \Omega}{A_2}\dfrac{\gamma(\omega r_m)}{a^2}\dfrac{\mathrm{d}P^*}{\mathrm{d}t^*} - \left(\dfrac{\gamma(\omega r_m)^2}{a^2}P^* + 1\right)\phi_p = -\phi_l \\ \dfrac{L}{r_m}\dfrac{\Omega}{\omega}\dfrac{\mathrm{d}\phi_l}{\mathrm{d}t^*} = P^* + c_x \end{cases} \tag{4}$$

where ϕ_l is a local flow coefficient calculated based on the axial velocity of the flow in the turbine duct, and c_x a non-dimensional coefficient for the aerodynamic axial turbine force. Equation (4) represents a system of 2 first order non-linear ordinary differential equations with P^* and ϕ_l representing the unknowns and ϕ_p the external forcing. c_x (the turbine axial force coefficient) needs to be provided as a function of other working parameters. Ghisu *et al.* [17] demonstrated, by means of CFD simulations, how in Wells turbines (at the non-dimensional frequencies typical of common operation), aerodynamic forces are a univocal function of the local flow coefficient (i.e. hysteretic effects are negligible). Figure 1 reports the turbine force coefficients derived from [17], which have been approximated using a first and a second order polynomial functions, respectively:

$$c_x = -c_{x,\phi}\phi_l \qquad T^* = t_0 + t_1\phi_l + t_2\phi_l^2 \tag{5}$$

Equation (4) can be converted to a single second order differential equation:

$$\frac{L}{r_m}\frac{\Omega}{\omega}\frac{\mathrm{d}^2\phi_l}{\mathrm{d}t^{*2}} + c_{x,\phi}\frac{\mathrm{d}\phi_l}{\mathrm{d}t^*} + \frac{a^2}{\gamma(\omega r_m)(h_1\Omega)}\frac{A_2}{A_1}\phi_l = \frac{a^2}{\gamma(\omega r_m)(h_1\Omega)}\frac{A_2}{A_1}\left(1 + \frac{\gamma(\omega r_m)^2}{a^2}P^*\right)\phi_p \tag{6}$$

In order to be solved analytically, equation (6) needs to be linearized. This can be done by assuming:

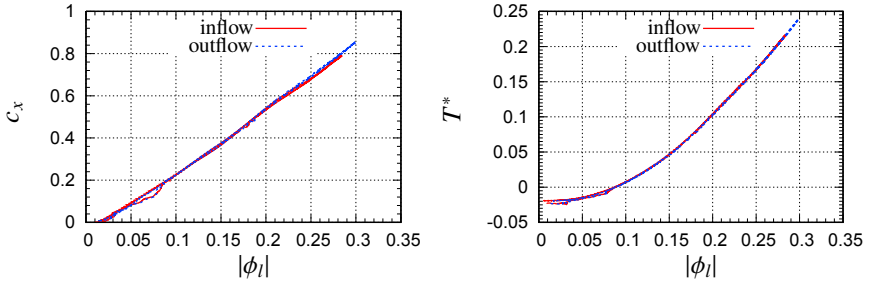

Fig. 1: Axial force coefficient and torque coefficient as function of local flow coefficient [17]

$$h_1 \approx h_{10} \text{ (its value at rest)} \qquad \left(1 + \frac{\gamma(\omega r_m)^2}{a^2} P^*\right) = \frac{\rho_1}{\rho_0} \approx 1 \tag{7}$$

After linearization, equation (6) becomes:

$$\underbrace{\frac{L}{r_m}\frac{\Omega}{\omega}}_{A}\frac{\mathrm{d}^2\phi_l}{\mathrm{d}t^{*2}} + \underbrace{c_{x,\phi}}_{B}\frac{\mathrm{d}\phi_l}{\mathrm{d}t^*} + \underbrace{\frac{a^2}{\gamma(\omega r_m)(h_{10}\Omega)}\frac{A_2}{A_1}}_{C}\phi_l = \underbrace{\frac{a^2}{\gamma(\omega r_m)(h_{10}\Omega)}\frac{A_2}{A_1}}_{D}\phi_p \tag{8}$$

The solution to equation (8) can be seen in terms of its transfer function $G(s^*)$, where $s^* = j$ is the Laplace variable:

$$G(s^*) = \frac{\phi_l}{\phi_p} = \frac{D}{As^{*2} + Bs^* + C} = \frac{\frac{D}{C}}{\frac{A}{C}s^{*2} + \frac{B}{C}s^* + 1} = \frac{\frac{D}{C}}{\left(\frac{\Omega}{\Omega_n}\right)^2 s^{*2} + 1 + 2\zeta\left(\frac{\Omega}{\Omega_n}\right)s^*} \tag{9}$$

In the above equations, Ω_n is the angular natural frequency and ζ the (non-dimensional) damping ratio of the system:

$$\Omega_n = \sqrt{\frac{C}{A}}\Omega = \sqrt{\frac{1}{h_{10}L}\frac{A_2}{A_1}\frac{a}{\gamma}} \qquad 2\zeta = \frac{B}{C}\frac{\Omega_n}{\Omega} = \frac{B}{C}\sqrt{\frac{C}{A}} = \frac{B}{\sqrt{AC}} = \frac{c_{x,\phi}}{\sqrt{\frac{L}{\gamma h_{10}}\frac{A_2}{A_1}\frac{a}{\omega r_m}}} \tag{10}$$

The solution to equation (8) is therefore:

$$\phi_l = \phi_{l0}\, e^{jt^* + \xi} \tag{11}$$

where:

$$\phi_{l0} = |\phi_l| = |\phi_p||G(s^*)| = \phi_{p0}|G(s^*)| \tag{12}$$

$$\phi_p = \phi_{p0}\, e^{jt^*} \tag{13}$$

$$|G(s^*)| = \frac{\frac{D}{C}}{\sqrt{\left[\left(-\frac{\Omega}{\Omega_n}\right)^2 + 1\right]^2 + \left[2\zeta\left(\frac{\Omega}{\Omega_n}\right)\right]^2}} = \frac{D}{\sqrt{(C-A)^2 + B^2}} \tag{14}$$

$$\xi = \tan^{-1}\left(\frac{-2\zeta\frac{\Omega}{\Omega_n}}{-\left(\frac{\Omega}{\Omega_n}\right)^2 + 1}\right) = \tan^{-1}\left(\frac{-B}{C-A}\right) = \tan^{-1}\left(\frac{c_{x,\phi}}{\frac{L}{r_m}\frac{\Omega}{\omega} - \frac{a^2}{\gamma(\omega r_m)(h_{10}\Omega)}\frac{A_2}{A_1}}\right) \tag{15}$$

Equation (15) deserves some attention. Because of the damping produced by the first order term in equation (8) (the resistance produced by the turbine), a delay exists between piston movement and mass-flow in the turbine duct.

3. Results

Figure 2 reports a comparison between the piston-based flow coefficient ϕ_p and the local flow coefficient ϕ_l during a period of piston movement. A small phase shift exists, caused by the resistive effect of the turbine Although small, this phase shift is enough to generate a hysteresis when turbine forces are presented as a function of piston-based flow coefficient ϕ_p, as in Figure 3. A good agreement between LPM, CFD (from [17]) and experimental data is found.

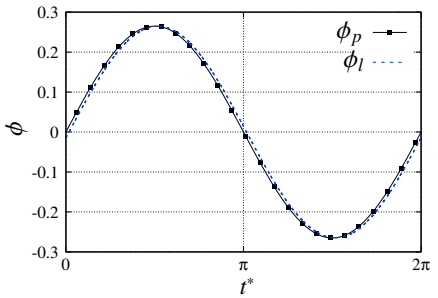

Fig. 2: Piston-based and local flow coefficient for $\sigma = 0.57$

The results obtained with the lumped parameter model are in good agreement with CFD and experimental data for the prediction of non-dimensional torque coefficient T^*; the maximum value of pressure drop coefficient is slightly un-

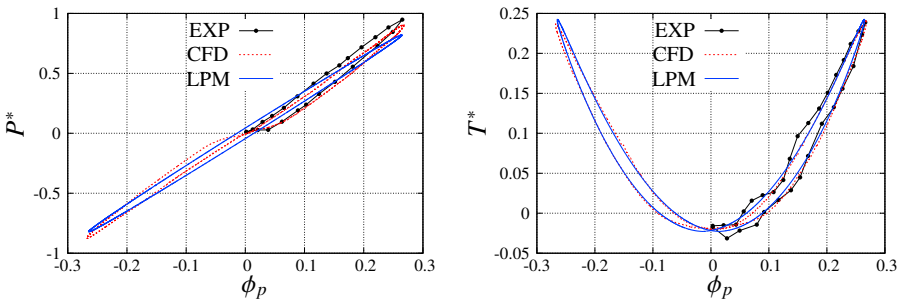

Fig. 3: Non-dimensional coefficient of pressure drop and torque for $\sigma = 0.57$: LPM approach compared with CFD and experimental data.

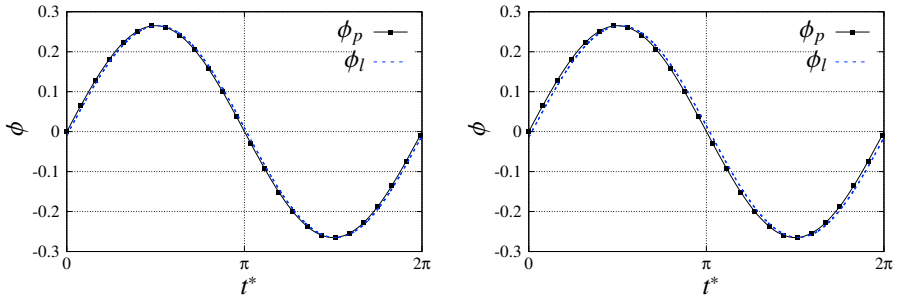

Fig. 4: Piston-based and local flow coefficient for $\sigma = 0.48$ (left) and $\sigma = 0.67$ (right)

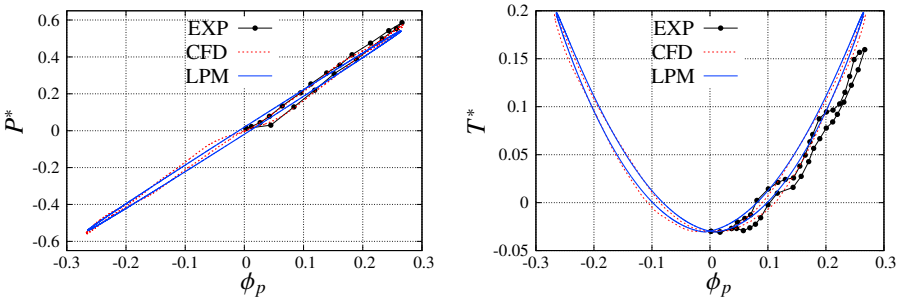

Fig. 5: Non-dimensional coefficient of pressure drop and torque: LPM approach compared with CFD and experimental data for $\sigma = 0.48$

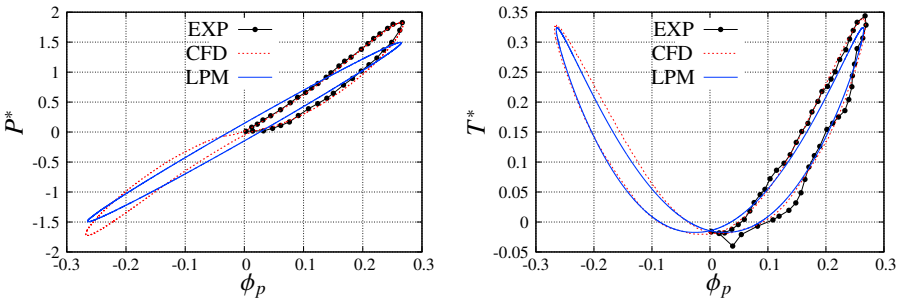

Fig. 6: Non-dimensional coefficient of pressure drop and torque: LPM approach compared with CFD and experimental data for $\sigma = 0.67$

derestimated if compared with CFD and experimental data. The hysteresis is well reproduced with the LPM approach, providing a further evidence that its origin is to be found in the capacitive behavior of the OWC system.

A further investigation has been done for two additional values of solidity ($\sigma = 0.48$ and $\sigma = 0.67$), while keeping the same system geometry and operating conditions used in the $\sigma = 0.57$ case. Higher values of solidity produce a larger axial turbine force and consequently larger $c_{x,\phi}$ and a larger phase shift between system forcing and system response. This is evident when comparing the piston-based flow coefficient ϕ_p with the local flow coefficient ϕ_l for the two new solidity values (Figure 4). A larger phase shift leads also to a larger system hysteresis when turbine force coefficients are presented as a function of the external forcing, i.e. the piston-based flow coefficient ϕ_p, as shown in Figures 5 and 6.

4. Conclusions

This work presents a lumped parameter model for the analysis of the interaction between an OWC system and a Wells turbine. It is shown that the system behaves as a second-order-system, with the turbine axial force providing the damping that is responsible for the delay between external forcing (water column movement) and system output

(mass-flow through the turbine duct). This analysis corroborates the results of recent CFD analyses that proved how the renowned Wells turbine hysteresis is in fact not a aerodynamic hysteresis of the turbine (unlikely at the non-dimensional frequencies it operates at), but a hysteresis of the overall OWC system.

The results obtained show an excellent agreement with experiential data and CFD analyses, making of the proposed model an ideal candidate for including turbine effects on overall more complex OWC system analyses.

References

[1] L. M. C. Gato, M. Webster, An experimental investigation into the effect of rotor blade sweep on the performance of the variable-pitch Wells turbine, Vol. 215, 2001, pp. 611–622.

[2] M. Takao, T. Setoguchi, S. Nagata, K. Toyota, A study on the effects of blade profile and non-uniform tip clearance of the Wells turbine, in: Proceedings of the 27th International Conference on Offshore Mechanics and Arctic Engineering, Vol. 6, 2008, pp. 625– 632. doi:10.1115/OMAE2008-57235.

[3] A. Thakker, P. Frawley, E. Sheik Bajeet, A. Heffernan, Experimental investigation of CA9 blades on a 0.3m wells turbine rig, in: Proceeedings of the Tenth (2000) International Offshore and Polar Engineering Conference, Vol. 8(1), Seattle, USA, 2000, pp. 1098–6189.

[4] Y. Kinoue, T. Setoghuci, T. H. Kim, K. Kaneko, M. Inoue, Mechanism of hysteretic characteristics of wells turbine for wave power conversion, Journal of Fluids Engineering, Transaction of the ASME 125 (2) (2003) 302–307. doi:10.1115/1.1538629.

[5] M. Takao, T. Setoguchi, K. Kaneko, S. Yu, Performance of wells turbine with guide vanes for wave energy conversion, Journal of Thermal Science 5 (2) (1996) 82–87. doi:doi.org/10.1007/s11630-996-0002-1.

[6] T. Setoguchi, M. Takao, K. Kaneko, Hysteresis on Wells turbine characteristics in reciprocating flow, International Journal of Rotating Machinery 4 (1) (1998) 17–24. doi:10.1155/S1023621X98000025.

[7] T. S. Dhanasekaran, M. Govardhan, Computational analysis of performance and flow investigation on Wells turbine for wave energy conversion, Renewable Energy 30 (14) (2005) 2129–2147. doi:10.1016/j.renene.2005.02.005.

[8] A. Gareev, P. Cooper, P. B. Kosasih, CFD analysis of air turbines as power take-off systems in oscillating water column wave energy conversion plant 2 analysis of linear aerofoil cascades, in: Proceedings of the 8th European Wave and Tidal Energy Conference (EWTEC), Uppsala, Sweden, 2009, pp. 777–785.

[9] M. Torresi, S. Camporeale, G. Pascazio, Detailed CFD analysis of the steady flow in a Wells turbine under incipient and deep stall conditions, Journal of Fluids Engineering, Transactions of the ASME 131 (7) (2009) 0711031–07110317. doi:10.1115/1.3155921.

[10] M. Nazeryan, E. Lakzian, Detailed entropy generation analysis of a Wells turbine using the variation of the blade thickness, Energy 143 (2018) 385–405. doi:10.1016/j.energy.2017.11.006.

[11] T. Setoguchi, Y. Kinoue, T. H. Kim, K. Kaneko, I. M, Hysteretic characteristics of Wells turbine for wave power conversion, Renewable Energy 28 (13) (2003) 2113–2127. doi:10.1016/S0960-1481(03)00097-X.

[12] M. Mamun, Y. Kinoue, T. Setoguchi, K. Kaneko, Hysteretic characteristics of the Wells turbine in a deep stall condition, Vol. 218, 2004, pp. 167–173. doi:10.1243/1475090041737967.

[13] Y. Kinoue, M. Mamun, T. Setoguchi, K. Kaneko, Hysteretic characteristics of Wells turbine for wave power conversion (effects of solidity and setting angle), International Journal of Sustainable Energy 26 (1) (2007) 51–60. doi:10.1080/14786450701359117.

[14] M. Paderi, P. Puddu., Experimental investigation in a wells turbine under bi-directional flow, Renewable Energy 57 (2013) 570–576. doi:10.1016/j.renene.2013.02.016.

[15] P. Puddu, M. Paderi, C. Manca, Aerodynamic Characterization of a Wells Turbine under Bi-directional Airflow, Energy Procedia 45 (2014) 278–287. doi:10.1016/j.egypro.2014.01.030.

[16] T. Ghisu, P. Puddu, F. Cambuli, Numerical analysis of a wells turbine at different non-dimensional piston frequencies, Journal of Thermal Science 24 (6) (2015) 535–543. doi:10.1007/s11630-015-0819-6.

[17] T. Ghisu, P. Puddu, F. Cambuli, Physical explanation of the hysteresis in Wells turbines: A critical reconsideration, Journal of Fluids Engineering, Transaction of the ASME 138 (11) (2016) 1–9. doi:10.1115/1.4033320.

[18] T. Ghisu, P. Puddu, F. Cambuli, I. Virdis, On the hysteretic behaviour of Wells turbines, Energy Procedia 126 (2017) 706–713. doi:10.1016/j.egypro.2017.08.303.

[19] T. Ghisu, P. Puddu, F. Cambuli, A detailed analysis of the unsteady flow within a Wells turbine, in: Proceedings of the Institution of Mechanical Engineers, Part A: Journal of Power and Energy, Vol. 231, 2017, pp. 197–214. doi:10.1177/0957650917691640.

[20] T. Ghisu, P. Puddu, F. Cambuli, N. Mandas, P. Seshadri, G. Parks, Discussion on “Performance analysis of Wells turbine blades using the entropy generation minimization method” by Shehata, A. S., Saqr, K. M., Xiao, Q., Shahadeh, M. F. and Day, A., Renewable Energy 118 (2018) 386–392. doi:10.1016/j.renene.2017.10.107.

[21] L. W. Carr, K. W. McAlister, W. J. McCroskey, Analysis of the development of dynamic stall based on oscillating airfoil experiments, Tech. Rep. NASA Technical Note D-8382, NASA AMES Research Center (1977).